Mesostructured fluids: a geometrical model predicting experimental data

Pascal André,[a] Barry W. Ninham[b,c] and Marie Paule Pileni*[a]

[a] *Laboratoire des Matériaux Mésoscopiques et Nanométriques (CNRS URA 1662), Université P. et M. Curie, B.P. 52, 4 Place Jussieu, 752 31 Paris cedex 05, France. E-mail: pileni@curie.sri.jussieu.fr*
[b] *Department of Applied Mathematics, Australian National University, P.O. Box 4, Canberra, ACT 0200, Australia*
[c] *Physical Chemistry I, University of Lund, P.O. Box 124, SE 22100 Lund, Sweden*

Received (in Montpellier, France) 10th November 2000, Accepted 6th December 2000
First published as an Advance Article on the web 19th March 2001

A geometrical model describing reverse micellar systems has been developed. A single phase containing assembled structures on two different length scales is described and the hydration of surfactants involved in each structure determined. By taking into account the water–surfactant interface a transition from interconnected cylinders to spheres has been predicted and is confirmed by experimental data. Furthermore, interdigitation between reverse micelles can be predicted and observed experimentally.

Emulsions are extremely important for a variety of industrial applications[1] or fundamental research.[2] Not only their stability, but also their microstructures are critical properties in these two fields. The microstructure of mixtures containing surfactant, oil and water has been the subject of many discussions.[3,4] For example, as recently as a decade ago some of the most active workers in the field of complex fluids held that supra-aggregated structures did not exist. Furthermore, as a matter of definition, emulsions have always been regarded as thermodynamically unstable systems.[5]

Two kinds of theories have been developed to predict the structure of ternary microemulsions under static conditions. The first considers the water–oil interface stabilized by a surfactant as a continuous film.[6,7] The behavior is then driven by the geometry of the structure. The curvature energies can be calculated and then optimization leads to predictions of topological transitions. The second type of theory considers the non-continuous nature of an interface composed of surfactants.[8] The geometry of the interface and that of the surfactant have to be considered. In this way, the expected spontaneous curvature corresponds to the energetically favorable packing configuration of the surfactant at the interface. The structure of micellar aggregates[8,9] is determined by the surfactant parameter, $s = v_s/a_s l_s$, where v_s, a_s and l_s are the volume of the surfactant, the surface area and the length of the alkyl chain, respectively. Spherical micelles are observed if $s < 1/3$, polydisperse rod shapes or globular micelles if $s < 1/2$, single walled vesicles or bilayers if $s < 1$ and reverse structures if $s > 1$. These two classes of theory can be refined by taking into account electrostatic interactions between two films or polar head groups for ionic surfactants.

Many structures can be envisaged in amphiphilic systems. Spheres, cylinders, spherulites or lamellae are a few examples, in addition interconnection can be taken into account. Each can pack in several ways: simple cubic, fcc *etc.* Packing imposes a limited amount of oil, water and surfactant inside an elementary cell. In a zero order model, oil, water and surfactant volume fractions are linked together due to the packing parameter, α_p.

In the oil-rich region, the phase diagram of $Cu(AOT)_2$–isooctane–water[10–12] has been carefully studied. At low water content, the various structures are governed by the hydration of the polar head group with a progressive increase in the s parameter. In the region where the polar head group should be totally hydrated there are thermodynamically stable "supra"-aggregates, made of an onion lamellar phase containing bicontinuous microemulsions in both its internal and external phases. From these data, it was concluded that the concept of "phase" in mesostructured fluids is too restrictive.

The samples were prepared as follows: $Cu(AOT)_2$ was mixed with isooctane and water progressively added. The solutions were sealed and vigorously shaken. The final emulsions and the equilibrium phases can be obtained by centrifugation or by standing for several minutes. These are reversible in temperature cycling and so each experimental emulsion is thermodynamically stable. The solutions are Newtonian,[13] as indicated by viscosity measurements,[10] thus the equilibrium phases are not influenced by the initial shaking.

In the present paper the geometrical model previously described is extended and applied to $Cu(AOT)_2$–water–isooctane solutions.[10–12] Quantitative calculations to predict structures differing in their packing are presented. For the supra-aggregates, it is possible to differentiate the hydration of the surfactants involved in the various structures composing the phase. Finally, at high water content, geometrical considerations can be used to predict a transition from interconnected cylinders to spheres, whereas at low water content the inverse transition is not predictable only due to geometrical arguments. Similarly, interdigitation involving reverse micelles can be predicted and experimentally observed.

The geometrical model

The parameters are defined in the Glossary. Packing of spheres and interconnected cylinders is governed by the packing parameter, α_p. Fig. 1(A)–(C) show the various pack-

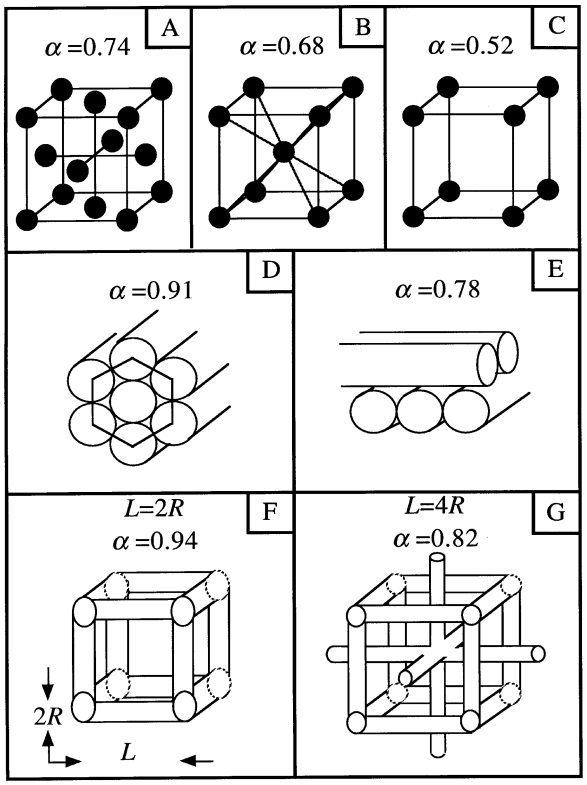

Fig. 1 Various packing of spheres: (A) face centered cubic (fcc), (B) body centered cubic (bcc), (C) simple cubic (sc). Organizations of cylinders: (D) hexagonal, (E) square, (F) interconnected cubic, (G) interconnected face centered cubic.

ings of spheres whereas Fig. 1(D)–(F) are those of interconnected cylinders.

To predict colloidal structure, the following parameters have to be taken into account: (i) the overall volume of a micelle including water, surfactant and "bound" oil, (ii) the volume of water trapped inside the colloid, and (iii) the internal surface area of the colloid assuming all the surfactant is located at the water–oil interface. Whatever the colloidal structure, packing is possible if the sum of volume fractions is less than the packing parameter α_p:

$$\phi_o^b + \phi_s + \phi_w < \alpha_p \quad (1)$$

where ϕ_o^b, ϕ_s, ϕ_w are the bound oil, surfactant and water volume fractions, respectively.

Packing of spheres and cylinders

The parameters governing the packing are the specific water content, $\bar{w}$, the surfactant parameter, s, and the packing parameter, α_p. In a previous paper,[11] we demonstrated that the limiting volume fractions of spherical micelles are:

$$\phi_s < \alpha_p \frac{3(3\bar{w}s)^2 s}{(3\bar{w}s+1)^3} = X_s \quad (2)$$

By replacing the packing parameter α_p with its various values (see Glossary), the limiting volume fractions are deduced for every kind of packing (sc, fcc, bcc, *etc.*). For simplicity, only the surfactant volume fraction and surfactant–oil volume fraction ratio are presented. The other ones can easily be deduced.

Similarly, the packing of infinite cylinders (square, hexagonal close packed) characterized per unit length is:

$$\phi_s < \alpha_p \frac{4\bar{w}s^2}{(2\bar{w}s+1)^2} = X_s \quad (3)$$

The packing parameter is not known for interconnected cylinders. It is calculated in Appendix A for simple cubic and fcc structures.

Packing conditions of interconnected cylinders in a simple cubic structure. The water volume inside an elementary cell is given by:

$$V_w = (3\pi L - 8\sqrt{2}\,R_w)R_w^2 = N_w v_w \quad (4)$$

Let l be the length between two interconnections, then the internal surface is:

$$S = R_w[2\pi(R_w + 3l) + 8R_w(1-\sqrt{2})] = N_s a_s \quad (5)$$

These equations lead to the cylinder water pool radius equation:

$$(6\pi - 8\sqrt{2})R_w^2 + \{3\pi l - [2\pi + 8(1-\sqrt{2})]\bar{w}sl_s\}R_w - 6\pi\bar{w}sl_s l = 0 \quad (6)$$

The total volume of the cell [Fig. 1(F)] is:

$$N_s v_s + N_o v_o + N_w v_w = L^3 = (2R_w + l)^3 \quad (7)$$

Once eqn. (6) is solved, the limiting ratio of oil and surfactant volume fractions is obtained from eqn. (7):

$$\frac{\phi_o}{\phi_s} = \frac{(2R_w + l)^3}{R_w\{R_w[2\pi + 8(1-\sqrt{2})] + 6\pi l\}} \frac{a_s}{v_s} - (\bar{w}+1) \quad (8)$$

From eqn. (8), the volume fraction limits for each component (surfactant, water and oil) can be deduced. The surfactant volume fraction is:

$$\phi_s < \frac{R_w\{R_w[2\pi + 8(1-\sqrt{2})] + 6\pi l\}}{(2R_w + l)^3} sl_s = X_s(l = 2l_s) \quad (9)$$

X_s, the surfactant limiting volume fraction of interconnected cylinders in simple cubic structures is obtained when $l = 2l_s$.

For a surfactant volume fraction greater than X_s, the interconnected cylinders have to evolve into a denser structure.

Packing conditions of interconnected cylinders in an fcc structure. The water volume and interfacial area are twice those in interconnected simple cubic structures and the total volume of the cell [Fig. 1(G)] is:

$$N_s v_s + N_o v_o + N_w v_w = L^3 = (4R_w + l)^3 \quad (10)$$

This relation leads to the surfactant volume fraction:

$$\phi_s < \frac{4R_w\{R_w[7\pi + 4(1-\sqrt{2})] + 3\pi l\}}{(4R_w + l)^3} sl_s = X_s(l = 2R_w + 4l_s) \quad (11)$$

The above equations are general and can be used for any surfactant. Nevertheless, some elementary behavior and parameters have to be known: the volume of water, v_w, and the polar head group area, a_s, as a function of the water content, the volume, v_s, and the length, l_s, of the surfactant hydrophobic part.

To support the model described above, comparison between the model and experimental data is made by using the $Cu(AOT)_2$–water–isooctane phase diagram. It is assumed also that the specific volume of water molecules and the polar head group area of $Cu(AOT)_2$ behave as a Na(AOT) solution. These hypotheses are needed to develop the model because no structural data for $Cu(AOT)_2$ are available at low water content. This assumption is supported by the fact that, at high water content, the polar head group area per surfactant is similar to that obtained with Na(AOT).[14,15] To a first approximation, it is assumed that the water molecule volume and the surface area increase logarithmically in the water content

range of 1 to 20.[3,15] Oil penetration, in the double chain or in the space between two surfactant molecules, could swell the hydrophobic part of the surfactant but this has not been taken into account. This is quite justified if the oil chain length is equal to or shorter than that of the surfactant. In the numerical applications, the surfactant is assumed to have a constant volume (639 Å^3)[16] and alkyl chain length (10 Å). In the formalism developed above and based on the volume fractions, the geometrical constraints impose the structure and the resulting packing limits are shown in a ternary diagram [Fig. 2(A)]. On increasing the surfactant concentration, the system evolves from spheres to infinite cylinders and then to interconnected cylinders.

Let us consider data in a given region of the phase diagram. $Cu(AOT)_2$ is solubilized in isooctane and a rather low amount of water is added ($0 < w < 5$). An isotropic phase is formed. On increasing water content above $w = 5$, a phase transition takes place and the isotropic phase coexists with isooctane.

(i) At water content, $w = 4$, and $[Cu(AOT)_2]_0 = 4.2 \times 10^{-1}$ M, one isotropic phase is formed. In our previous papers,[11,12,14,17] it was demonstrated from SAXS and conductivity measurements that interconnected cylinders are formed. This is at point A in the phase diagram in Fig. 2(B). The surfactant and water volume fractions are 0.30 and 0.06, respectively. From the various packing limits shown in Fig. 2(B), spheres cannot pack in sc and bcc structures whereas this is possible in an fcc structure. Packing of interconnected cylinders is possible whatever the packing structure is. These results are consistent with the experimental data.

(ii) At $w = 2$ and $[Cu(AOT)_2]_0 = 4.2 \times 10^{-1}$ M, the SAXS experiments and the low conductivity make it possible to conclude that there is formation of spherical reverse micelles. This corresponds to point B in the phase diagram given in Fig. 2(B). The surfactant and water volume fractions are 0.31 and 0.04, respectively. From Fig. 2(B), it is clear that spheres can no longer pack and must transit to elongated cylinder-like objects. Taking into account this fact, it can be deduced that cylinders are probably formed. However, the packing structure (square, fcc, hexagonal) cannot be discerned. The difference between experimental data and the model can be attributed to the fact that the system used is highly concentrated. Formation of spheres from SAXS measurements was deduced from simulation of both the structure factor and the form factor with a hard sphere potential. Furthermore, it is difficult to differentiate by SAXS between polydispersed spheres and elongated aggregates. The low conductance could be due to the fact that the water molecules are more tightly bound to the interface. Taking into account experimental data and the model, it can be concluded that the high surfactant-to-water ratio forces the surfactant tails to line up, as it would for stacking of a "Chinese fan".

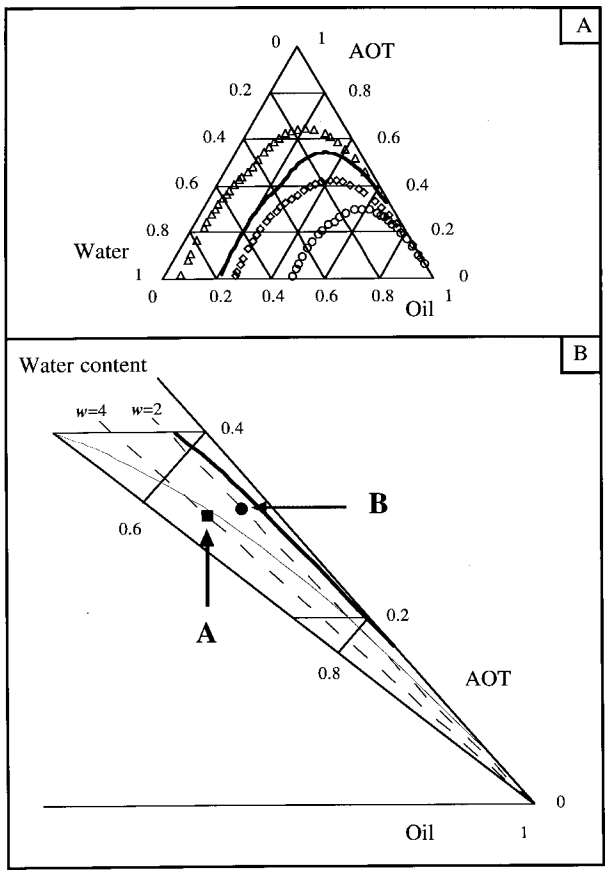

Fig. 2 Ternary diagram in volume determined for constant AOT chain length, surfactant and oil volumes. (A) Packing limits for cylindrical structures: (△) interconnected simple cubic, (——) square; packing limits for spherical structures: (◇) face centered cubic, (○) simple cubic. (B) Packing limits at low water content in the oil-rich region (see text for description of points A and B): (——) spheres in face centered cubic structure, (———) cylinders in square structure.

At $w = 5$, a phase transition is observed and oil is released from the surfactant chains. The upper phase is isooctane whereas the lower phase is interconnected cylinders. It has been shown previously that such phase transitions are interaction dependent.[18] This transition cannot be predicted by geometrical considerations. Indeed, the progressive increase in the water content causes hydration of the polar head group area. The consequence is a decrease in the surfactant parameter, s. However, this induces not only changes in the curvature of the oil–water interface, but also a change in the alkyl chain conformation and in the interactions. These have not been taken into account in the geometrical model and these could explain why this phase transition cannot be predicted by geometrical considerations only.

To summarize, the above equations give insight, in a very simple and general way, into the packing limits in a surfactant–water–oil system. The numerical results depend on the experimental parameters (a_s, v_s, v_w, *etc.*) introduced in the calculations. Nevertheless, except when interactions are too large, the experimental data are in good agreement with the model.

Supra-aggregates

$Cu(AOT)_2$ is solubilized in isooctane, $[(Cu(AOT)_2]_0 = 1.2 \times 10^{-1}$ M. Water is added to the solution to reach an overall water content, $w = [H_2O]/[AOT]$, in the range of $15.5 < w < 26$. The upper phase (1) is isotropic whereas the lower one (2) is birefringent. In our previous paper, we gave the characteristics of this region of the phase diagram.[17] In the following, we give a summary of the data obtained when increasing the overall water content from $w = 15.5$ to $w = 26$.

(i) An increase in the upper phase volume occurs whereas that of the lower phase decreases.

(ii) Increases in the water and AOT concentrations are observed. However, the water content of the upper phase, $w(1)$, remains constant and equal to 24. Conversely, the water and surfactant concentrations remain unchanged in the lower phase. This implies a constant average water content of the lower phase, $w(2) = 17$.

(iii) The SAXS pattern of the upper phase (1) shows a peak due to the structure factor. This peak slightly shifts toward large wave vector, q, values on increasing the overall water content. In the lower phase (2), the SAXS patterns drastically change with increasing overall water content. At low water content ($w = 17$), a large Bragg peak with a strong increase in the scattering intensity at low q values is observed. On increasing the overall water content, the Bragg peak shifts toward large q values, its width decreases and its intensity increases. This indicates an increase in the ordering of the

lamellar distance, d. Furthermore, on increasing the overall water content, a progressive emergence of a new peak in the same range of q values is observed in the upper phase (1).

(iv) The freeze fracture electron microscopy pattern of the upper phase is characterized by a small object [Fig. 3(A)] whereas the lower one is an onion phase with an internal small object [Fig. 3(B)].

These experimental data were explained in terms of self-assembled-supra-aggregate formation with an onion (or spherulite) phase containing interconnected cylinders in its external and internal phases. It is not a conventional emulsion. The system is considered as a single phase containing assembled structures on two different length scales. Furthermore, when the overall water content increases, the spherulite's interior collapses into an interconnected microemulsion. The whole system is in equilibrium. The lamellae, which separate interior and exterior phases, then adjust their spacing and component fractions to allow equilibration while keeping the water content constant in the two structures. Interlamellar forces dictate the amount of the components contained in these structures. This is strongly supported by the geometrical model described in our previous paper.[11,12,14,17] In addition, surfactants in the birefringent phase are involved to form either lamellae or interconnected cylinders.

At this point a question arises: does the hydration of the surfactant involved in the lamellae and in the interconnected cylinders remain similar to the birefringent phase overall water content, $w(2)$?

To answer this question, we have to take into account the experimental data published previously.[17] In the isotropic phase (1) made of interconnected cylinders, the characteristic distance, $D^* = 2\pi/q_{max}$, determined from the maximum of the peak due to the structure factor, is calculated at various water and surfactant volume fractions, $\phi_w(1)$, $\phi_s(1)$. In the birefringent phase, a peak is observed at a low q value and in the same range as the isotropic phase. It is assumed that this peak is due to the isotropic phase trapped inside the spherulites.

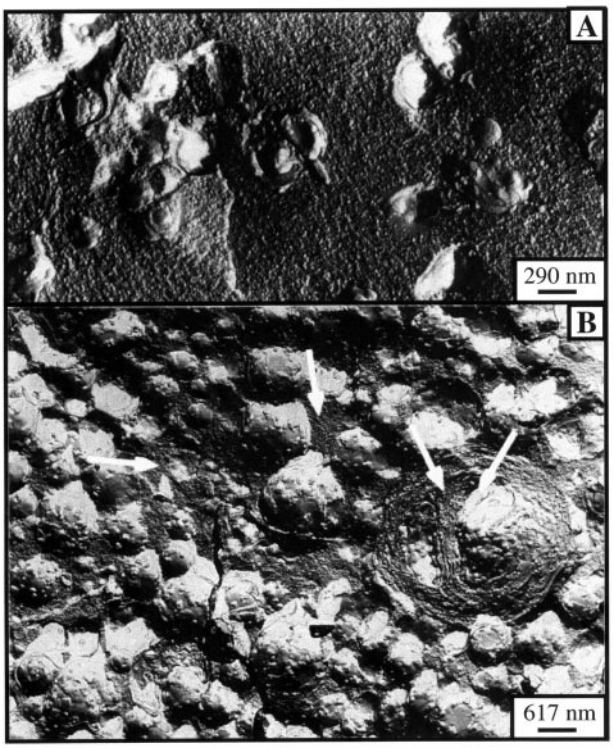

Fig. 3 Freeze fracture electron microscopy (FFEM) patterns. (A) Isotropic phase obtained at $w = 21$, $[Cu(AOT)_2]_0 = 4.2 \times 10^{-1}$ M (upper phase: $\phi_s = 0.21$, $\phi_w = 0.23$, $\phi_s = 0.56$). (B) Birefringent phase obtained at $w = 21$, $[Cu(AOT)_2]_0 = 4.2 \times 10^{-1}$ M (lower phase: $\phi_s = 0.30$, $\phi_w = 0.24$, $\phi_s = 0.46$).

From the value of its maximum and its characteristic distance, the water and surfactant volume fractions of the isotropic phase trapped in the spherulites are deduced, $\phi_w^1(2)$, $\phi_s^1(2)$. This enables us to determine the hydration, $w^1(2)$, of the surfactant involved in the interconnected cylinders present in the birefringent phase:

$$w^1(2) = \frac{\phi_w^1(2)}{\phi_s^1(2)} \frac{v_s}{v_w} \tag{12}$$

The hydration $w^1(2)$ is found to be similar to $w(1)$ [$w(1) = 24$, Table 1]. Furthermore, from the overall composition of the system, the total water and surfactant volume fractions, Φ_w and Φ_s, can be calculated. The overall water and surfactant volume fractions of the birefringent phase, $\phi_w(2)$ and $\phi_s(2)$, are obtained from the difference between the overall volume fraction and that due to interconnected cylinders. Taking into account the volume fraction of the interconnected cylinders in the biphasic system, f, leads to the following expression:

$$\phi_s(2) = [\Phi_s - f\phi_s(1)]/(1 - f) \tag{13}$$

The overall volume fraction of the birefringent phase is the sum of that due to lamellae, $\phi_w^{lam}(2)$ and $\phi_s^{lam}(2)$, and to the interconnected cylinders (*i.e.*, to the isotropic phase trapped in and between the spherulites), $\phi_w^1(2)$ and $\phi_s^1(2)$. Assuming that spherulites are packed in a simple cubic structure, their packing parameter is $\pi/6$. This is a crude approximation but the result should be independent of this. The surfactant volume fraction in the birefringent lamellae phase is then:

$$\phi_s^{lam}(2) = \left[\phi_s(2) - \left(1 - \frac{\pi}{6}\right)\phi_s^1(2)\right] \Big/ \frac{\pi}{6} \tag{14}$$

Table 1 gives the values of the various volume fractions deduced at various overall water contents. The hydration of the surfactant molecules involved in the lamellae, $w^{lam}(2)$ is proportional to the ratio of the water *vs.* surfactant volume fractions attributed to lamellae:

$$w^{lam}(2) = \frac{\phi_w^{lam}(2)}{\phi_s^{lam}(2)} \frac{v_s}{v_w} \tag{15}$$

Table 1 shows that the $w^{lam}(2)$ value does not change with increasing the overall water content. In this calculation, v_s is fixed at 639 Å^3, corresponding to the surfactant volume in reverse micelles.[16] However, in the present case, lamellae are formed and the surface curvature tends to change, that is the surfactant volume tends to decrease. Hence, the $w^{lam}(2)$ values given in Table 1 are overestimated. Nevertheless, for any v_s value, $w^{lam}(2)$ remains unchanged in the range of overall water content $15.5 < w < 26$).

The overall hydration of the birefringent phase [$w(2) = 17$] remains constant with increasing overall water content (Table 1). However, from these data it can be concluded that inside the birefringent phase the surfactant hydration is inhomogeneous, with $w^{lam}(2) = 13$ in the lamellar and $w^1(2) = 24$ in the interconnected cylindrical structures. This means that the number of water molecules used to solvate the surfactant differs with their self-organization. The model described above is simple but makes it possible to explain the experimental results with reasonably good accuracy. The validity of this approach was confirmed previously.[17] Actually, it has been possible to deduce the overall volume fractions of the system, taking into account the interlamellar distances determined by SAXS and the volume fractions of the upper phase determined by titration. Good agreement between experimental data and the geometrical model is obtained.

Microemulsion region

In the region of the phase diagram corresponding to a fairly large amount of water ($29 < w < 40$), the solution of $Cu(AOT)_2$–water–isooctane is isotropic and the head

Table 1 Experimental data obtained for a $Cu(AOT)_2$–water–isooctane system with $[Cu(AOT)_2]_0 = 4.2 \times 10^{-1}$ M[a]

w	17	18	19	20	21	22	23	24
$\phi_s(1)$	—	0.17	0.18	0.19	0.21	0.22	0.23	0.24
$\phi_w(1)$	—	0.19	0.20	0.22	0.23	0.25	0.27	0.27
$D^*(1)$/Å	157	157	157	146	127	125	125	121
$w(1)$	—	23.5	23.8	23.9	22.9	23.9	24.5	24.8
$\phi_s(2)$	—	0.28	0.29	0.29	0.30	0.30	0.27	0.26
$\phi_w(2)$	—	0.21	0.23	0.23	0.24	0.24	0.22	0.21
$D^*(2)$/Å	—	—	157	140	126	125	125	125
$w(2)$	—	16.3	16.6	16.7	17.5	17.3	17.5	17.8
$\phi_s^1(2)$	—	—	0.18	0.20	0.22	0.23	0.23	0.23
$\phi_w^1(2)$	—	—	0.19	0.22	0.25	0.26	0.26	0.26
$\phi_s^{lam}(2)$	—	—	0.39	0.36	0.33	0.34	0.29	0.26
$\phi_w^{lam}(2)$	—	—	0.26	0.23	0.22	0.22	0.18	0.17
$w^1(2)$	—	—	22.9	23.6	24.2	24.2	24.2	24.2
$w^{lam}(2)$	—	—	14.1	13.9	14.4	13.9	13	13.7

[a] w is the overall water content. (1) and (2) indicate isotopic and birefringent phases, respectively. ϕ_s and ϕ_w are the surfactant and water volume fractions. $w(1)$ and $w(2)$ are the mean water content of the isotropic and birefringent phases, deduced from titration. $w^1(2)$ and $w^{lam}(2)$ are water contents of cylinders and lamellae in the birefringent phase. $D^*(Å) = 2\pi/q_{max}$ where q_{max} is the maximum of the scattering intensity.

group area (55 $Å^2$) is constant. A careful study based on SAXS data, conductivity measurements and freeze fracture electron microscopy shows that the microemulsion evolves, upon increasing the water content from $w = 29$ to 40, from interconnected cylinders to isolated spheres. The transition takes place at $w = 32$. This transition is rather surprising. The reverse is usually expected with the geometrical model [Fig. 2(A)] based on the volume fraction values. To explain such behavior, the water–surfactant interface for both interconnected cylinders and spherical structures has to be considered. The water radius, R_w, is defined: (i) for a sphere as the water pool radius and (ii) for a cylinder as its half width. The surface of a sphere is proportional to its radius squared. The calculation of the surface of interconnected cylinders is not trivial. Connections between cylinders have to be taken into account. Details of the calculation concerning the surface of interconnected cylinders are given in Appendix A and depends on the radius, R_w, and on the length, L, of the cylinders.

For packing in a simple cubic structure the surface is given by replacing [in eqn. (5)] the length between two interconnections, l, with the length of the cylinders, L:

$$S = R_w[2\pi(3L - 5R_w) + 8R_w(1 - \sqrt{2})] \quad (16)$$

The L value is that determined by SAXS measurements and is 150 Å.[14] The increase in the water content induces an increase in the R_w value. The water–oil surface of spheres continuously increases whereas that of interconnected cylinders increases to reach a plateau and then decreases (Fig. 4). This involves constraints that drastically increase with increasing water content. Because of such constraints, the system self arranges into a structure having fewer connections but more interfaces. The surfactant obtains more freedom to rearrange. Such behavior explains the transition from interconnected cylinders to spheres. The intersection between the variation with R_w of the surface due to interconnected cylinders and spheres takes place at $R_w = 60$ Å. This corresponds to the water pool radius observed just above the structural transition (at $w = 32$). This is in good agreement with experimental data that show a transition from interconnected cylinders to spheres at $w = 32$. This simple model explains quantitatively the transition from interconnected cylinders to spheres of $Cu(AOT)_2$–water–isooctane around $w = 32$.

In the region where spherical water-in-oil droplets are formed ($w > 32$), we could ask what happens when the excess of oil is not sufficient to accommodate the curvature required by the surfactant chains. This occurs on increasing the surfactant concentration. Oil cannot fill up the gaps between objects and the spheres must digitate. The geometrical conditions to reach interdigitated reverse micelles are given by the limiting value of the oil-to-surfactant volume fraction ratio, ϕ_0/ϕ_s.

Let us assume that spheres are packed in a simple cubic structure [Fig. 1(C)]. This provides the equivalence of a single droplet and the elementary cell of the array. The equations are much more complicated for bcc, fcc or random packing.

When interdigitation of spheres occurs, the volume of the cell is:

$$(2R_w + l_s)^3 < N_w v_w + N_s v_s + N_o v_o \leqslant (2R_w + 2l_s)^3 \quad (17)$$

Interdigitated reverse micelles are obtained when:

$$\frac{\phi_o}{\phi_s} \leqslant \frac{(6\bar{w}s + 2)^3}{\pi s(6\bar{w}s)^2} - (\bar{w} + 1) = \frac{X_o}{X_s} \quad (18)$$

By plotting ϕ_o/ϕ_s *vs.* the water content for $Cu(AOT)_2$–water–isooctane solution, the upper limit to reach interdigitated reverse micelles is found, as shown in Fig. 5. The lower limit is obtained when:

$$\frac{\phi_o}{\phi_s} > \frac{(6\bar{w}s + 1)^3}{\pi s(6\bar{w}s)^2} - (\bar{w} + 1) \quad (19)$$

Fig. 5 clearly shows the limits corresponding to free and interconnected reverse micelles. At large ϕ_o/ϕ_s values the reverse micelles are free whereas at lower values they are interdigitated. At very low ϕ_o/ϕ_s values, the distance between micelles is lower than the chain length of the surfactant. This makes any interdigitation impossible.

At $[Cu(AOT)_2]_0 = 4.2 \times 10^{-1}$ M, the interdigitation limit is reached. The diamonds in Fig. 5 represent the ϕ_o/ϕ_s values measured at various water contents. At a lower $Cu(AOT)_2$ concentration (1.2×10^{-1} M), free reverse micelles are formed (see dots in Fig. 5). Changes from free to interdigitated reverse micelles can be observed by high resolution freeze fracture electron microscopy. At low $Cu(AOT)_2$ concentration, small

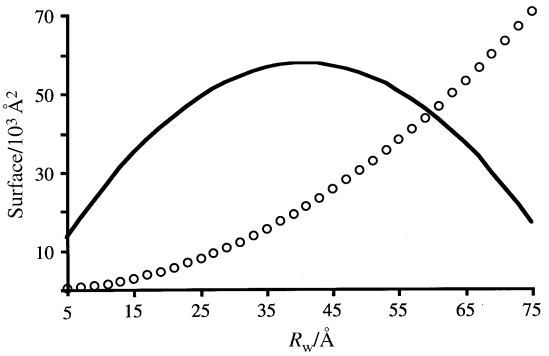

Fig. 4 Interfacial surfaces calculated for (○) spheres and (——) interconnected cylinders in the simple cubic structure, keeping L fixed at 150 Å.

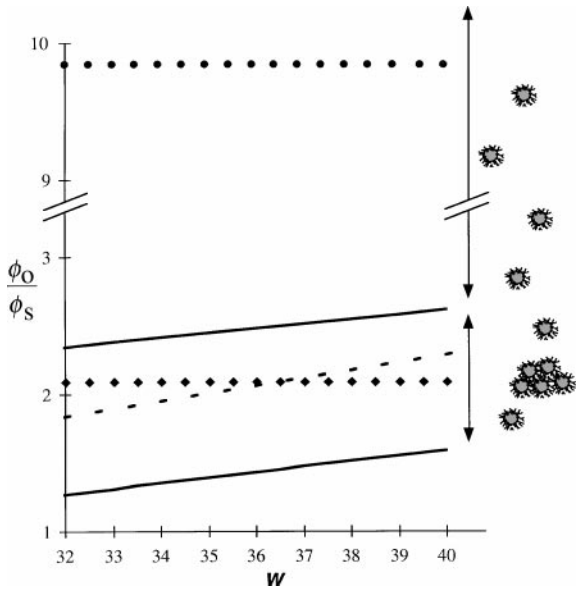

Fig. 5 Variation of the volume fraction ratio of oil and surfactant for reverse micelles in sc structure with water content. The region above the upper solid line corresponds to reverse isolated micelles. The region between the solid lines corresponds to spherical interdigitated micelles. The region below the dotted line and above the solid line corresponds to a mixture of spherical and flattened ($\theta = \pi/5$) interdigitated water-in-oil droplets. Experimental single phase having $[Cu(AOT)_2]_0$ (◆) 4.2×10^{-1} M and (●) 1.2×10^{-1} M.

objects with an average size of around 10 nm are observed [Fig. 6(A)] whereas coexistence between large and small objects is obtained at high $Cu(AOT)_2$ concentration (4.2×10^{-1} M), as shown in Fig. 6(B).

Hence interdigitated reverse micelles can be formed, above $w = 32$, by increasing $Cu(AOT)_2$ concentration. Fig. 7(A) shows, in a ternary diagram, a large domain in which the interdigitated reverse micelles exist.

Another question arises: does the shape of reverse micelles change from spherical to an elementary cell flattened at the faces? Appendix B describes the calculation to determine the ϕ_o/ϕ_s ratio limit, below which the shape of interdigitated reverse micelles changes. It is:

$$\frac{\phi_o}{\phi_s} = \frac{\left(6\bar{w}s\,\frac{B(\theta)}{A(\theta)} + 1\right)^2}{\pi s(6\bar{w}s)^2 B(\theta)^3} A(\theta)^2 - (\bar{w} + 1) \qquad (20)$$

where θ is the angle of a cap cut-off, when spherical reverse micelles are flattened on the six faces of the unit cell (Fig. 8).

The variation of the ϕ_o/ϕ_s ratio with water content is plotted in Fig. 5 (dotted line). Above the dotted line, spherical interdigitated droplets are formed whereas below this line the droplets are flattened at their faces. From the experimental data, a change from spheres to faceted reverse micelles is expected around $w = 36$. It should be noted that these calculations were made for simple cubic packing.

For infinite cylinders in square structures, a similar calculation gives the upper limit to observe the interdigitation process. It takes place when the oil and surfactant volume fraction ratio is:

$$\frac{\phi_o}{\phi_s} \leqslant \frac{(2\bar{w}s + 1)^2}{\pi\bar{w}s^2} - (\bar{w} + 1) = \frac{X_o}{X_s} \qquad (21)$$

Interdigitation takes place when the oil and surfactant volume fraction ratio is higher than:

$$\frac{\phi_o}{\phi_s} > \frac{(4\bar{w}s + 1)^2}{4\pi\bar{w}s^2} - (\bar{w} + 1) \qquad (22)$$

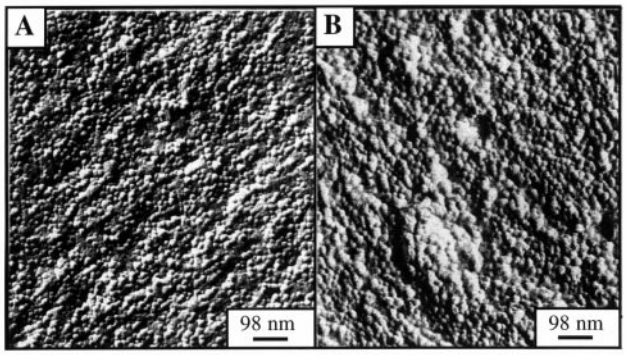

Fig. 6 FFEM patterns. (A) Microemulsion obtained at $w = 40$ and $[Cu(AOT)_2]_0 = 1.2 \times 10^{-1}$ M ($\phi_s = 0.08$, $\phi_w = 0.15$, $\phi_s = 0.77$). (B) Microemulsion obtained at $w = 40$ and $[Cu(AOT)_2]_0 = 4.2 \times 10^{-1}$ M ($\phi_s = 0.20$, $\phi_w = 0.38$, $\phi_s = 0.42$).

When the interdigitation cannot increase further, the system evolves to denser packing or phases separate. The region of interdigitated cylinders in a square structure is shown in Fig. 7(B). Interconnected cylinders can be observed in a very concentrated regime. This explains why it has been impossible to observe them in dilute solution, which has been explored in the $Cu(AOT)_2$–water–isooctane system.

Conclusion

We have developed a simple geometrical model in order to predict structural transitions and supra-aggregation processes in reverse amphiphilic systems. It is focused on the surfactant parameter, volume fractions and hydration. It gives an overview of constraints imposed by geometrical packing and their influence on microemulsion structures. These results are quite general and qualitatively in good agreement with experimental behavior. We have shown that phase behavior and microstructures can be described and predicted by algebra with

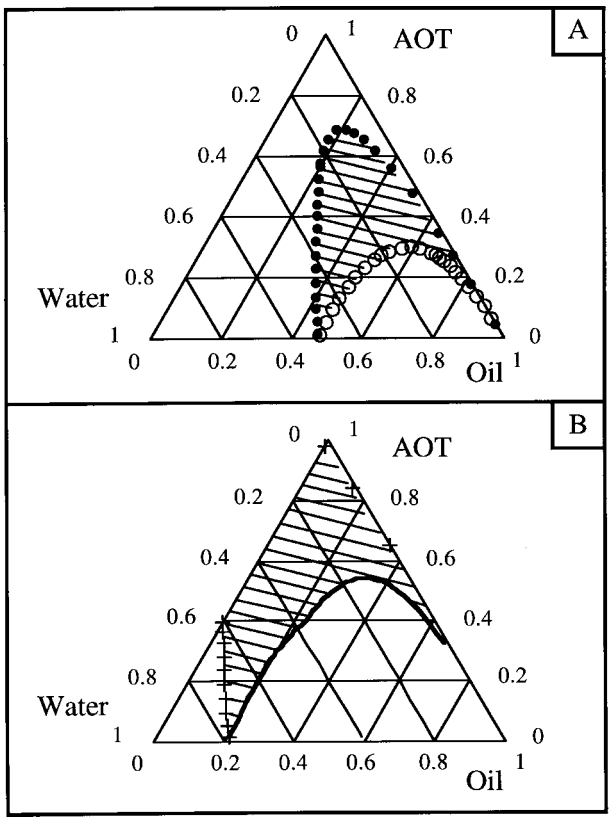

Fig. 7 (A) (○) Packing and (●) interdigitation limits for spherical micelles in simple cubic structures. The interdigitation region is between the two curves. (B) (——) Packing and (++) interdigitation limits for cylindrical micelles in square structures.

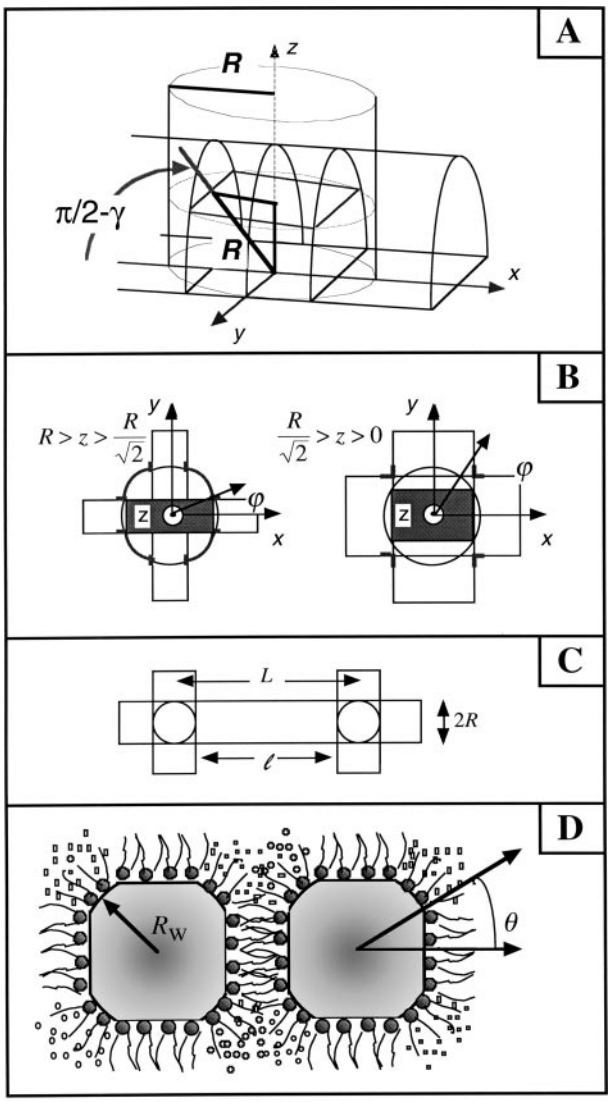

Fig. 8 Interconnection of cylinders of radius R. (A) Interconnection of two perpendicular cylinders. The angle φ gives the height of the interconnection of two cylinders parallel to the Ox and Oz axes. (B) Interconnection of three perpendicular cylinders. The angle ϕ describes, in the xOy plane, the interconnection of two cylinders parallel to the Ox and Oz axes. (C) L is the cylinder length and l is the distance between two interconnections. (D) Schematic of interdigitated micelles flattened at their faces with θ the angle of the flat faces.

elementary geometry describing local and global packing conditions, without statistical mechanics or any kind of interaction. This is simultaneously the quality and the defect of the model.

The generality we claim can be expected to occur in biological systems where compartmentalization of reactants is universal. Our point is that the complexity of such systems may have a simple origin beyond the dismissal of complexity in the term "non equilibrium thermodynamics".

Acknowledgements

The authors would like to thank A. Filankembo, Dr I. Lisiecki and Dr C. Petit (LMMN). Thanks are also due to Dr T. Gulik-Krzywicki of the Centre de Génétique Moléculaire (CNRS) at Gif-sur-Yvette.

Appendix A: interconnected cylinders volumes and surfaces

Packing calculations for interconnected structures require more attention. In order to establish the volume fraction limits of each component, the volume and surface of the structure inside the elementary cell have to be determined.

Let us consider the intersection of two cylinders characterized by an orthogonal point (Ox, Oy, Oz). R and z are the radius and the height of the cylinders, respectively. The z value is $z = R\cos\gamma$, where γ gives the height of the interconnection of two cylinders parallel to the Ox and Oz axes, respectively [Fig. 8(A)]. The z value can vary between 0 and R. The angle φ describes, in the xOy plane, the interconnection of the same two cylinders parallel to the Ox and Oz axes [Fig. 8(B)].

An elementary cell formed by three interconnected cylinders and characterized by a volume V_1 is considered. This elementary cell is a cube having a size equal to the length of the cylinder, L. It corresponds to the center-to-center distance between intersections [Fig. 8(C)]. To determine V_1 we have to take into account the volume of each cylinder ($3\pi R^2 L$), that of the intersection of two V_2 and of three V_3 cylinders, respectively. Taking into account all these volumes:

$$V_1 = 3\pi R^2 L - 3V_2 + V_3 \tag{A1}$$

The intersection volume of two cylinders, V_2, is the surface shared between the two cylinders, given by the integration of:

$$V_2 = 2\int_0^R S(z)\mathrm{d}z = 2\int_0^R 2R^2(\cos\varphi\,\sin\varphi + \varphi)\mathrm{d}(R\cos\varphi) \tag{A2}$$

The cylindrical symmetry [Fig. 8(A) and (B)] sets $\varphi = \gamma$, varies between $[\pi/2; 0]$. Integration leads to:

$$V_2 = \tfrac{16}{3}R^3 \tag{A3}$$

The intersection volume of three cylinders, V_3, is the surface shared between three cylinders, given by the integration of:

$$\begin{aligned} V_3 &= 2\int_0^{R/2} 4R^2\left(\sin\varphi_1\cos\varphi_1 + \frac{\pi}{4} - \varphi_1\right)\mathrm{d}z \\ &\quad + 2\int_{R/2}^{R} 4R^2\sin^2\varphi\,\mathrm{d}z \\ V_3 &= 2\int_0^{R/2} 4R^2\left(\sin\varphi\cos\varphi + \frac{\pi}{4} - \varphi\right)\mathrm{d}z \\ &\quad + 2\int_{R/2}^{R} 4R^2\sin^2\varphi\,\mathrm{d}z \end{aligned} \tag{A4}$$

φ_1 and φ give the height of the interconnection of two cylinders parallel to the Ox and Oz axes, for $z < R/\sqrt{2}$ and $z > R/\sqrt{2}$, respectively. There are discriminated for convenience. The cylindrical symmetry sets $\gamma = \varphi = (\pi/2) - \varphi_1$. φ and φ_1 vary between $[\pi/4; 0]$ and $[0; \pi/4]$, respectively.

$$V_3 = 8R^3(2 - \sqrt{2}) \tag{A5}$$

In an sc structure, the volume of interconnected cylinders in an elementary cell is:

$$V_1 = (3\pi L - 8\sqrt{2}\,R)R^2 \tag{A6}$$

The packing parameter, α_p, is determined for simple cubic and fcc structures.

Simple cubic structure

The volume fraction of interconnected cylinders is the ratio of the volume really occupied by the cylinders and that of the elementary cell:

$$\alpha_p = \frac{(3\pi L - 8\sqrt{2}\,R)R^2}{L^3} \tag{A7}$$

The maximum volume occupied by the cylinders is obtained when they are in contact, that is when $L = 2R$. The packing parameter is then:

$$\alpha_p = \tfrac{3}{4}\pi - \sqrt{2} \simeq 0.94 \quad \text{(A8)}$$

Interconnected cylinders in fcc structures

The internal volume is twice that of an sc structure. The volume fraction of interconnected cylinders is:

$$\alpha_p = \frac{2(3\pi L - 8\sqrt{2}\,R)R^2}{L^3} \quad \text{(A9)}$$

The packing parameter of interconnected cylinders in fcc structures is obtained at contact, $L = 4R$:

$$\alpha_p = \frac{3\pi - 2\sqrt{2}}{8} \simeq 0.82 \quad \text{(A10)}$$

$$S_i = \int_0^{\pi/4} [8(1 - \cos\varphi) + (2\pi - 8\varphi)]R \, dz + \int_{\pi/4}^{\pi/2} 8R(1 - \sin\varphi)dz \quad \text{(A11)}$$

The cylindrical symmetry sets $\gamma = \varphi$. The integration, realised between $[\pi/2; 0]$, leads to:

$$S_i = 2R^2[\pi + 4(1 - \sqrt{2})] \quad \text{(A12)}$$

To determine the water–surfactant surface, the length l [Fig. 8(C)] between two cylinders without intersection is considered. The internal surface of interconnected cylinders is the sum of the surface of each cylinder and that of the interconnection. The intersection surface of three cylinders is calculated by integration of the shared perimeter:
The surface of interconnected cylinders in an sc structure inside an elementary cell is given by the following relation:

$$S = R[2\pi(R + 3l) + 8R(1 - \sqrt{2})] \quad \text{(A13)}$$

If l, the length between two intersections, is replaced by $L = l - 2R$, the length of the interconnected cylinders, eqn. (A13) leads to the equivalent relation:

$$S = R[2\pi(3L - 5R) + 8R(1 - \sqrt{2})] \quad \text{(A14)}$$

In fcc structures, the internal surface of interconnected cylinders is also twice that of sc structures.

Appendix B: volume and surface of interdigitated droplets flattened at their faces

On decreasing the amount of oil, spherical water droplets could change in shape and reach a flattened structure. Hence, the spheres progressively flatten at the faces of the Wigner–Seitz cell.

Let us assume a simple cubic packing of spherical droplets flattened at their faces. With a water core radius, R_w, the angle of the cap, θ and γ the angle of integration, the volume of a cap cut-off, V_1, is:

$$V_1 = \int_{R\cos\theta}^{R} \pi(R_w \sin\gamma)^2 d(R_w \cos\gamma) \quad \text{(B1)}$$

$$V_1 = \frac{\pi}{3} R_w^3[2(1 - \cos\theta) - \cos\theta \sin^2\theta] \quad \text{(B2)}$$

Then the water volume inside of the droplet is:

$$V_w = N_w v_w = \frac{4\pi}{3} R_w^3 - 6V_1 \quad \text{(B3)}$$

The area of a cap is:

$$S_1 = \int_0^{\theta} 2\pi R_w^2 \sin\gamma \, d\gamma = 2\pi R_w^2(1 - \cos\theta) \quad \text{(B4)}$$

The area of a flattened region is:

$$S_2 = \pi(R_w \sin\theta)^2 \quad \text{(B5)}$$

The total area at the surface interface is:

$$S = 4\pi R_w^2 - 6S_1 + 6S_2 \quad \text{(B6)}$$

The water–oil interface is totally covered with the surfactants, so:

$$N_s a_s = 4\pi R_w^2[\tfrac{3}{2}(2 - \cos\theta)\cos\theta - \tfrac{1}{2}] \quad \text{(B7)}$$

The water volume inside the droplet, $V_w = N_w v_w = (4\pi/3)R_w^3 - 6V_1$, and eqn. (B7) lead to the water core radius expression:

$$R_w = 3\bar{w}sl_s \frac{3(2 - \cos\theta)\cos\theta - 1}{3(3 - \cos^2\theta)\cos\theta - 4} \quad \text{(B8)}$$

The cell is made of interdigitated alkyl chains. Taking into account that the total volume in the elementary cell is:

$$N_w v_w + N_s v_s + N_o v_o = (2R_w \cos\theta + l_s)^3 \quad \text{(B9)}$$

gives eqn. (B10) for the limiting ratio of oil and surfactant volume fractions:

$$\frac{\phi_o}{\phi_s} = \frac{\left(6\bar{w}s \dfrac{B(\theta)}{A(\theta)} + 1\right)^3}{\pi s(6\bar{w}s)^2 B(\theta)^3} A(\theta)^2 - (\bar{w} + 1) \quad \text{(B10)}$$

with $A(\theta) = \tfrac{3}{2}(3 - \cos^2\theta)\cos\theta - 2$ and $B(\theta) = \tfrac{3}{2}(2 - \cos\theta) - \cos\theta - \tfrac{1}{2}$ where R_w is the water core radius and θ the angle of flat faces.

Fig. 5 shows the various limits to reach the zones of isolated droplets, interdigitated spherical or interdigitated flattened spherical and droplets.

Glossary

Number of oil, water and surfactant molecules: N_o, N_w, N_s
Water and surfactant concentration: C_s, C_w
Avogadro number: $\mathcal{N}_0$
Volume of the studied phase, φ: V_φ
Volume of oil, water and of the AOT surfactant molecule:[16] v_o, v_w and v_s (=639 Å^3)
Surfactant volume fraction: $\phi_s = C_s \mathcal{N}_0 v_s = \dfrac{N_s v_s}{V_\varphi}$
Water volume fraction: $\phi_w = C_w \mathcal{N}_0 v_w = \dfrac{N_w v_w}{V_\varphi}$
Oil volume fraction: $\phi_o = \dfrac{N_o v_o}{V_\varphi} = 1 - (\phi_s + \phi_w)$
Bound oil volume fraction: ϕ_o^b
Water content: $w = \dfrac{N_w}{N_s}$
Specific water content: $\bar{w} = \dfrac{\phi_w}{\phi_s} = \dfrac{N_w v_w}{N_s v_s}$
Surfactant alkyl chain length: $l_s = 10$ Å
Polar head group area: a_s, $a_s(\max) = 55$ Å^2
Surfactant parameter: $s = s(w) = \dfrac{v_s}{a_s(w)l_s}$
Maximum volume fraction of packing: α_p

Shape	Structure	α_p
Spheres	Simple cubic	$\dfrac{\pi}{6} \approx 0.52$
Spheres	Body centered cubic	$\dfrac{\sqrt{3}\pi}{8} \approx 0.68$
Spheres	Face centered cubic	$\dfrac{\pi}{3\sqrt{2}} \approx 0.74$
Cylinders	Hexagonal close compact	$\dfrac{\pi}{2\sqrt{3}} \approx 0.91$

Cylinders	Square structures	$\frac{\pi}{4} \approx 0.78$
Interconnected cylinders	Simple cubic	0.94
Interconnected cylinders	FCC structure	0.82

Volume fraction limit: X
Water core radius: R_w
Interior volume of a micelle: V_w
Surfactant chain volume per micelle: V_s
Bound oil volume: V_o^b
Volume fraction of the isotropic phase (upper phase): f
Volume fraction of the birefringent phase (lower phase): $1-f$
Overall system volume fractions of oil, water and surfactant: Φ_o, Φ_w and Φ_s
Surfactant volume fraction of the isotropic phase, $\phi_s(1)$, inside the isotropic one
Surfactant volume fraction of the isotropic phase, $\phi_s^1(2)$, inside the birefringent one
Surfactant volume fraction in lamellar structure, $\phi_s^{lam}(2)$, inside the birefringent phase
Length of interconnected cylinders cell: L
Length between two interconnections: l
Flat face angle of a spherical micelle: θ
Scattering wave vector in SAXS measurements: q

References

1 *Emulsion and Emulsion Technology*, ed. K. J. Lissant, Marcel Dekker, New York, 1974, vol. 6.
2 *Micelles, Microemulsions and Monolayers: Science and Technology*, ed. D. O. Shah, Marcel Dekker, New York, 1998.
3 *Reactivity in Reverse Micelles*, ed. M. P. Pileni, Elsevier, Amsterdam, 1989.
4 S. Hyde, S. Andersoon, K. Larsson, Z. Blum, T. Landh, S. Lidin and B. W. Ninham, *The Language of Shape*, Elsevier, Amsterdam, 1997.
5 J. Bibette, D. C. Morse, T. A. Witten and D. A. Weitz, *Phys. Rev. Lett.*, 1992, **69**, 2439.
6 T. Tlusty, S. A. Safran and R. Strey, *Phys. Rev. Lett.*, 2000, **84**, 1244.
7 W. M. Gelbart and A. J. Ben-Saul, *J. Phys. Chem.*, 1996, **100**, 13169.
8 J. N. Israelachvili, D. J. Mitchell and B. W. Ninham, *J. Chem. Soc., Faraday Trans. 2*, 1976, **72**, 1525.
9 D. J. Mitchell and B. W. Ninham, *J. Chem. Soc., Faraday Trans. 2*, 1981, **77**, 601.
10 J. Tanori, T. Gulik-Krzywicki and M. P. Pileni, *Langmuir*, 1997, **13**, 632.
11 I. Lisiecki, P. André, A. Filankembo, C. Petit, J. Tanori, T. Gulik-Krzywicki, B. W. Ninham and M. P. Pileni, *J. Phys. Chem.*, 1999, **103**, 9168.
12 I. Lisiecki, P. André, A. Filankembo, C. Petit, J. Tanori, T. Gulik-Krzywicki, B. W. Ninham and M. P. Pileni, *J. Phys. Chem.*, 1999, **103**, 9176.
13 H. Hoffman and A. Rauscher, *Colloid Polym. Sci.*, 1993, **271**, 390.
14 A. Filankembo, P. André, I. Lisiecki, C. Petit, T. Gulik-Krzywicki, B. W. Ninham and M. P. Pileni, *Colloids Surf., A*, 2000, **174**, 221.
15 L. Motte, I. Lisiecki and M. P. Pileni, in *Hydrogen Bond Networks*, ed. J. Dore and M. C. Bellisan, NATO, London, 1994, p. 447.
16 M. Magalhaes, D. Pusiol, E. Ramia and A. M. Figueiredo Neto, *J. Chem. Phys.*, 1998, **108**, 3835.
17 P. André, A. Filankembo, I. Lisiecki, C. Petit, T. Gulik-Krzywicki, B. W. Ninham and M. P. Pileni, *Adv. Mater.*, 2000, **12**, 119.
18 S. A. Safran, L. A. Turkevich and P. A. Pincus, *J. Phys. Lett.*, 1984, **45**, L69.